International Journal of Radiation Oncology biology • physics

www.redjournal.org

Physics Contribution

# Near Real-Time Assessment of Anatomic and Dosimetric Variations for Head and Neck Radiation Therapy via Graphics Processing Unit–based Dose Deformation Framework

X. Sharon Qi, PhD,* Anand Santhanam, PhD,* John Neylon, MS,* Yugang Min, PhD,* Tess Armstrong, BS,* Ke Sheng, PhD,* Robert J. Staton, PhD,† Jason Pukala, PhD,† Andrew Pham, MD,* Daniel A. Low, PhD,* Steve P. Lee, MD, PhD,* Michael Steinberg, MD,† Rafael Manon, MD,† Allen M. Chen, MD,* and Patrick Kupelian, MD*

**Department of Radiation Oncology, University of California Los Angeles, Los Angeles, California; and †Department of Radiation Oncology, UF Health Cancer Center - Orlando Health, Orlando, Florida*

Received Aug 15, 2014, and in revised form Jan 16, 2015. Accepted for publication Jan 27, 2015.

**Summary**

Nearly real-time assessment of anatomic and dosimetric consequences for head and neck treatment is feasible using a graphics processing unit–based deformable registration framework. Substantial interfraction anatomic changes resulting in clinically relevant dosimetric variations were observed for 11 head and neck cases. Although the cumulative target mean and maximum doses varied insignificantly, the cumulative minimum

**Purpose:** The purpose of this study was to systematically monitor anatomic variations and their dosimetric consequences during intensity modulated radiation therapy (IMRT) for head and neck (H&N) cancer by using a graphics processing unit (GPU)-based deformable image registration (DIR) framework.

**Methods and Materials:** Eleven IMRT H&N patients undergoing IMRT with daily megavoltage computed tomography (CT) and weekly kilovoltage CT (kVCT) scans were included in this analysis. Pretreatment kVCTs were automatically registered with their corresponding planning CTs through a GPU-based DIR framework. The deformation of each contoured structure in the H&N region was computed to account for nonrigid change in the patient setup. The Jacobian determinant of the planning target volumes and the surrounding critical structures were used to quantify anatomical volume changes. The actual delivered dose was calculated accounting for the organ deformation. The dose distribution uncertainties due to registration errors were estimated using a landmark-based gamma evaluation.

**Results:** Dramatic interfractional anatomic changes were observed. During the treatment course of 6 to 7 weeks, the parotid gland volumes changed up to 34.7%, and the center-of-mass displacement of the 2 parotid glands varied in the range of 0.9 to 8.8 mm. For the primary treatment volume, the cumulative minimum and mean and

Reprint requests to: X. Sharon Qi, PhD, UCLA, 200 Medical Plaza, Ste B265-95, Los Angeles, CA 90095. Tel: (310) 267-8982; E-mail: xqi@mednet.ucla.edu

This work was presented previously at the 55th Annual Meeting of the American Society for Radiation Oncology, Atlanta, GA, September 24, 2013. Year, and the 56th Annual Meeting of the American Association of Physicists in Medicine, Austin, TX, July 23, 2014.

Conflict of interest: none.

Int J Radiation Oncol Biol Phys, Vol. 92, No. 2, pp. 415–422, 2015
0360-3016/$ - see front matter 
http://dx.doi.org/10.1016/j.ijrobp.2015.01.033

target and parotid gland doses deviated significantly from the plans. Clinical implementation of this technology may enable timely plan adaptation and potentially lead to improved outcome.

equivalent uniform doses assessed by the weekly kVCTs were lower than the planned doses by up to 14.9% ($P=.14$), 2% ($P=.39$), and 7.3% ($P=.05$), respectively. The cumulative mean doses were significantly higher than the planned dose for the left parotid ($P=.03$) and right parotid glands ($P=.006$). The computation including DIR and dose accumulation was ultrafast (~45 seconds) with registration accuracy at the subvoxel level.

**Conclusions:** A systematic analysis of anatomic variations in the H&N region and their dosimetric consequences is critical in improving treatment efficacy. Nearly real-time assessment of anatomic and dosimetric variations is feasible using the GPU-based DIR framework. Clinical implementation of this technology may enable timely plan adaptation and improved outcome. 

## Introduction

Intensity modulated radiation therapy (IMRT) is a standard treatment technique for head and neck (H&N) cancer. IMRT has demonstrated the capability of delivering highly conformal doses to targets while sparing adjacent critical structures including parotid glands, spinal cord, and others. Daily volumetric image guidance not only improves patient alignment and dose delivery accuracy but also reveals patient anatomic changes resulting from patient weight loss, tumor shrinkage, soft tissue deformation, and internal organ motion (1, 2). These anatomic changes are commonly observed among H&N patients undergoing RT (1-5). If unaccounted for, the changes may have detrimental effects on tumor control and sparing of organs at risk (OARs) (1, 3, 4).

Adaptive RT (ART) is an appealing concept that aims to adjust the treatment plan based on the anatomical changes assessed on a daily basis, using pretreatment volumetric images (6-12). Wu et al (3) reported that the dosimetric benefit of replanning with reduced margins could result in up to 30% parotid gland dose sparing. Lee et al (4) reported an average of 15% difference between the mean dose to the parotid and that of the planned dose due to anatomic changes during a course of radiation treatment. Recently, Schwartz et al (9) performed a prospective adaptive trial for a group of 24 H&N cancer patients with 1 to 2 replan(s) in the middle of the treatment course. The early outcomes indicated promising clinical outcome results including low initial toxicity and high disease control. Chen et al (13) also concluded that ART confers a significant benefit in appropriately selected patients with H&N cancer. However, clinical implementation of ART remains challenging and labor intensive due to the complexity and lack of robustness in automated image registration, segmentation, and dose summation. Subsequently, the integration of ART in H&N treatment is mostly manual and empirical, without precise knowledge of the most appropriate timing and frequencies to initiate ART (1-4). A robust automated ART framework is essential to implement the concept in routine clinical workflow without inducing treatment delay or excessive staff burden.

We aimed to validate an in-house deformable image registration (DIR) and dose accumulation framework (14) that registered the patient's daily treatment scan to the planning computed tomography (CT) by using a patient-specific biomechanical H&N model and a multiresolution registration method with the following goals: (*1*) to enable fast assessment of the anatomic changes and organ motion for both targets and OARs during the course of treatment; and (*2*) to evaluate the resulting dosimetric differences between the delivered doses and the planned doses. Our ultimate goal was to monitor the delivered dose to the primary targets and critical structures in nearly real time and to facilitate a data-driven decision-making process for ART.

## Methods and Materials

### In-house graphics-based unit-based dose deformation and accumulation framework

The general-purpose graphics processing unit (GPU)-based framework involved mainly a multiresolution optical flow registration algorithm for registering simulation CTs with corresponding weekly CT datasets (14, 15). The computational steps were optimized to ensure the registration algorithm was completed in subminute computational time. First, the target volumes and OARs delineated on the planning CT were registered in a nonrigid manner and transferred to the weekly CT images. The deformation of each contoured structure was computed to account for nonrigid changes in the patient setup. Second, by warping the planning kilovoltage CT (kVCT) anatomy to the weekly anatomy, a new warped kVCT was generated. The planning dose distribution was then overlaid on the warped kVCT. To compute the dose delivered to each voxel in the planning volume, the deformation map was used to accumulate the overlaid dose back on the planning CT. This generated a new dose map that corresponded to the underlying anatomy in the weekly CT. The new contour was created automatically by taking each voxel in the new data volume and mapping it back to the planning CT, using the deformation vector. The deformed contours allowed for dose calculation and accumulation, resulting in dose-volume histograms (DVHs) and other dosimetric parameters. Third, the Jacobian determinant for the planning target volume (PTVs)

and the critical structures was used to quantify anatomical volume changes for each week. Fourth, a gamma analysis (7) was performed to provide a quantitative comparison between the calculated doses with respect to the planning dose distribution. The acceptance criteria for the gamma test were set to 1% intensity difference in 1-mm$^3$ range; gamma $\leq 1$ was considered acceptable.

### Landmark-based registration validation

The key to the work was the accuracy and robustness of the in-house registration algorithm. The validation of the proposed DIR framework, including the deformable image registration and the dose integration were performed using planning kV and weekly kV images. A landmark-based interactive validation tool was developed to evaluate the uncertainty in dose distribution due to registration error. We considered the planning kVCT to be the source (or reference) image and the final week of the weekly kVCT to be the target image. For each of the selected landmarks in the reference image, the corresponding landmark in the target kVCT data was calculated using the image registration algorithm and visually displayed as cross hairs in the target image. A set of 100 landmarks were selected on the target or critical structures of a reference kVCT and mapped to the target image. Once the landmarks were picked, the user either accepted the registration results or marked the correct landmark on the target image. The target registration error (TRE) metrics (14, 15), defined as the sum of the squared difference between the ground truth displacement and the displacement computed from the registration process for each of the datasets, were computed.

### Clinical data

Eleven H&N patients treated with simultaneous integrated boost technique on a Hi-ART tomotherapy system (Accuray Inc) were included to validate the in-house-developed framework. Patient data for this study were acquired as part of an institutional review board–approved adaptive planning protocol. All patients received 2 sets of volumetric image scans during treatment: weekly kVCTs and daily megavoltage CTs acquired before each treatment. The planning kVCT image set was acquired prior to the start of treatment, using a Brilliance CT system (Philips Medical Systems, Best, The Netherlands). Weekly volumetric kVCT images of each patient enrolled in the protocol were reacquired on the same equipment throughout the course of treatment. All patient kVCT images were acquired with the patient in the simulated treatment position using a 50- to 70-cm field of view, 512 × 512 pixels in-plane resolution, and 3-mm slice thickness. Table 1 shows the patient characteristics. A total of 71 weekly kVCT scans were acquired and analyzed. Patients 9, 10, and 11 (patient numbers are shown in Tables 1 and 2) were replanned during the middle of the treatment. Megavoltage CTs were not used in this study due to poorer soft tissue contrast. Unless otherwise specified, the accumulated doses were computed based on weekly kVCTs.

The prescription doses were 2.0 to 2.1 Gy/fraction delivered in 30 to 35 fractions. The targets and critical structures, such as clinical target volumes (CTVs), PTVs, spinal cord, and parotid glands were delineated by a radiation oncologist on the planning CT. A 3-mm margin was used for the CTV-to-PTV expansion, and a 5-mm margin was applied to the cord to account for setup uncertainty. All patients were treated with helical IMRT (version 4.1; TomoTherapy), with a field size of 2.5 cm, pitches of 0.277 to 0.3, and modulation factors of 2.2 to 3.2.

### Assessment of anatomic and dosimetric variations

The anatomic and positional changes for the targets and the parotid glands were measured on the weekly kVCT scans. For the targets, the delivered mean, minimum, and maximum dose, D90 (the minimum dose covering 90% of PTV), D95, V90 (the percent volume covering 90% of prescription dose), V95, and V100, as well as equivalent uniform dose (EUD) were calculated (assuming $\alpha = -15$ for the targets) and collected. For the OARs, we considered the minimum, mean, and maximum doses for the cord and parotid glands. The center of mass (COM) for the PTV1 and parotid glands and the COM distances between these structures were measured. Weekly delivered doses were estimated assuming constant anatomy for that week as reflected by the weekly kVCT. Finally, the accumulated dose was calculated and compared to the planned dose.

## Results

### Accuracy and robustness of the framework

Figure 1 shows the verification of the in-house DIR framework using a landmark tool. Figure 1a shows the source image (the planning CT) with delineated structure outlines of the target and left and right parotids. Figure 1b and c show the target image (a weekly kVCT) overlaid with the deformed contours. The corresponding landmark points in the target image were calculated using the image registration algorithm and visually displayed as cross hairs.

Table 2 shows the registration accuracy and the standard deviation of the whole body, the PTV, and the left and right parotids, using a landmark-based TRE metric (14). The averaged TREs were in the range of 0.88 to 1.25 mm (average: 1.03 ± 0.72 mm), 0.68 to 2.42 mm (average: 1.34 ± 0.67 mm); 1.28 to 2.13 (average: 1.79 ± 0.89 mm); and 1.45 to 2.11 mm (average: 1.77 ± 0.85 mm) for entire patient anatomy, PTV, and left and right parotids, respectively. Given the pixel size of 1.95 × 1.95 × 3 mm, the proposed DIR framework reached subvoxel accuracy.

We further evaluated the dose distribution uncertainties due to registration errors. The landmark-based interactive

**Table 1** Patient characteristics and treatment delivery summary

| Patient | Diagnosis | No. of fx | Date enrolled (mo/d/y) | Tx beginning date (mo/d/y) | Tx completion date (mo/d/y) | Tx duration (d) | Initial weight (kg) | Final weight (kg) | Weight change (kg) |
|---|---|---|---|---|---|---|---|---|---|
| 1 | Nasopharynx | 33 | 06/23/11 | 06/23/11 | 08/09/11 | 47 | 81.6 | 76.2 | −5.4 |
| 2 | Tonsil | 35 | 11/17/11 | 11/17/11 | 12/30/11 | 43 | 93.4 | 83.8 | −9.6 |
| 3 | Tonsil | 35 | 11/25/09 | 12/07/09 | 01/26/10 | 50 | 88.0 | 85.9 | −2.1 |
| 4 | Tonsil | 35 | 04/23/09 | 05/07/09 | 07/02/09 | 56 | 95.7 | 84.8 | −10.9 |
| 5 | Tonsil | 35 | 10/20/10 | 10/28/10 | 12/20/10 | 53 | 72.1 | 63.3 | −8.8 |
| 6 | BOT | 35 | 12/29/10 | 01/07/11 | 02/18/11 | 51 | 63.5 | 62.6 | −0.9 |
| 7 | Tonsil | 35 | 08/17/09 | 08/31/09 | 10/09/09 | 39 | 83.9 | 76.9 | −7.0 |
| 8 | Tonsil | 30 | 10/08/12 | 10/16/12 | 11/28/12 | 43 | 86.4 | 82.0 | −4.4 |
| 9 | Tonsil | 35 | 11/21/11 | 11/21/11 | 01/05/12 | 45 | 107.5 | 96.0 | −11.5 |
| 10 | BOT | 35 | 10/18/12 | 10/22/12 | 12/11/12 | 50 | 99.8 | 89.1 | −10.7 |
| 11 | Ethmoid Sinus | 35 | 03/02/11 | 03/02/11 | 04/20/11 | 49 | 84.8 | 79.4 | −5.4 |

*Abbreviations:* BOT = base of tongue; fx = fraction; Tx = treatment.

tool was developed to evaluate the uncertainty of registration error. We modified the gamma dose distribution evaluation tool to quantify the effect of the spatial uncertainty of the deformable registration on dose distribution. Using the mean and standard deviation of the target registration error, we introduced a normally distributed random displacement during evaluation. For each voxel in the test dose distribution, the gamma analysis works by finding the corresponding voxel in the truth dose distribution, and performing a local neighborhood search to evaluate the Euclidean magnitude in dose/distance space. The random displacement was applied when finding the corresponding voxel in the truth-dose distribution, to effectively shift the local search neighborhood. The gamma analysis was then performed as usual. The introduction of random error caused less than 1% increase in the percentage of voxels that failed both the gamma evaluation (1%/1 mm) and a direct dose comparison.

**Table 2** Average ± SD registration accuracy across the entire body

| | Overall accuracy (mm) | | PTV accuracy (mm) | | Left parotid accuracy (mm) | | Right parotid accuracy (mm) | |
|---|---|---|---|---|---|---|---|---|
| Subject | Avg | ±SD | Avg | ±SD | Avg | ±SD | Avg | ±SD |
| 1 | 1.00 | 0.71 | 0.68 | 0.45 | 1.87 | 0.97 | 1.63 | 0.77 |
| 2 | 1.08 | 0.78 | 1.05 | 0.42 | 2.04 | 1.09 | 1.70 | 0.85 |
| 3 | 1.23 | 0.84 | 1.69 | 0.70 | 1.97 | 0.81 | 2.06 | 0.87 |
| 4 | 1.01 | 0.54 | 1.21 | 0.50 | 1.32 | 0.51 | 1.45 | 0.54 |
| 5 | 0.99 | 0.62 | 1.23 | 0.55 | 1.28 | 0.50 | 1.51 | 0.68 |
| 6 | 0.98 | 0.73 | 1.52 | 0.74 | 1.69 | 0.82 | 1.73 | 0.79 |
| 7 | 0.88 | 0.64 | 0.74 | 0.39 | 1.95 | 1.13 | 1.87 | 1.03 |
| 8 | 0.90 | 0.82 | 2.42 | 1.53 | 1.97 | 1.20 | 1.90 | 1.16 |
| 9 | 0.99 | 0.76 | 1.88 | 1.10 | 1.68 | 0.93 | 1.58 | 0.68 |
| 10 | 1.02 | 0.72 | 0.97 | 0.41 | 2.13 | 1.17 | 2.11 | 1.16 |
| 11 | 1.25 | 0.79 | 1.34 | 0.56 | 1.84 | 0.70 | 1.95 | 0.80 |

Multiple observers, including the primary physician, physician residents, and physicists reviewed the deformed contours for the target and parotid glands using the proposed landmark verification tool. Minimal variations (1-2 mm) of interobserver errors were found, which is comparable to the TRE metrics.

## Interfractional variations

The in-house tool was applied to analyze the patient cohort of 11 cases. The volume changes were assessed by weekly kVCT scans and normalized to the planning volume. The volume changes varied from −34.7% to 14.6% and −27.7% to 12.6%, respectively, for the left and right parotids during the 6- to 7-week treatment course. The volume increases between the planning week (week 0) CT to week-1 CT were likely due to the elapsed days between the planning CT and the start date of the first treatment (Table 1).

Figure 2a shows the contours of the parotid glands throughout the treatment course of 6 weeks for a representative patient. On average, the COM distances between the two parotid glands appeared to decrease in the range of 0.9 to 8.8 mm (mean: 4.9 ± 2.3 mm) at the end of the treatment course, meaning that the parotid glands were gradually moving toward the patient's mid-plane. Figure 2b and c show the COM distance (normalized to the COM distance at the planning stage) versus the ratio of the mean doses normalized to the planned mean doses for the parotid glands. The delivered mean doses increased as the parotid glands gradually migrated toward the mid-sagittal (high-dose region) plane. Linear regression was performed for the mean parotid gland doses as a function of COM displacement. Moderate correlation was observed between COM displacement and the mean parotid dose deviation from the plan. This observation was consistent with published reports (2, 4, 11, 12).

All patients lost weight over the treatment course (Table 1). The average and relative weight losses were

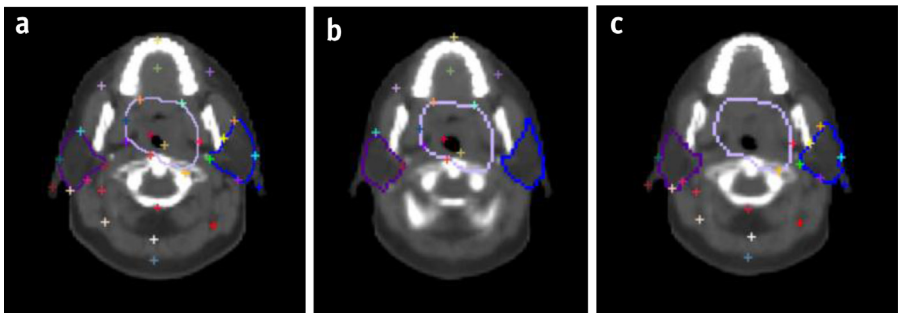


**Fig. 1.** Verification of in-house deformable image registration, using a landmark tool. (a) Source image with the delineated structures; (b and c) target image overlaid with the deformed contours. The selected landmark points in the source and target images were displayed as crosshairs.

7.0 ± 3.6 kg and 7.8% ± 3.7%, respectively. Given the treatment duration of 6 to 7 weeks, the weight-loss-per-treatment-elapsed days was approximately 0.14 ± 0.09 kg/day. Linear regression ($R^2 < 0.4$) shows there was mild correlation between patient weight loss and mean parotid dose change but no apparent correlation was found between the cord maximum dose, the PTV1 mean dose, and patient weight change (not shown).

The cumulative mean doses assessed by the weekly kVCT scans for the PTV1 were 68.9 ± 6.1 Gy versus 68.8 ± 6.2 Gy for the planned dose ($P = .39$ using paired t-tests). The maximum cord dose delivered was 43.7 ± 7.5 Gy compared to 40.7 ± 4.2 Gy ($P = .18$). However, significantly higher mean doses were seen for both parotid glands in the composite plans ($P = .03$ for the left parotid and $P = .006$ for the right parotid) shown in Figure 3a and b.

Figure 3d shows the ratio of the cumulative dose to the planned dose for the PTV1 in this patient cohort. While the maximum doses were consistent with the planned maximum doses within 5.7%, the cumulative mean dose ratios were within 1.1% of the planned mean doses for PTV1. Target DVHs also showed a moderate level of variation. Cold spots were observed in the cumulative dose distributions for the PTV1 in 6 out of 11 patients. Up to 14.9% of minimum dose reduction was observed for patient 7 (who had the second largest PTV volume), resulting in significant EUD changes ($P = .05$) from the plan.

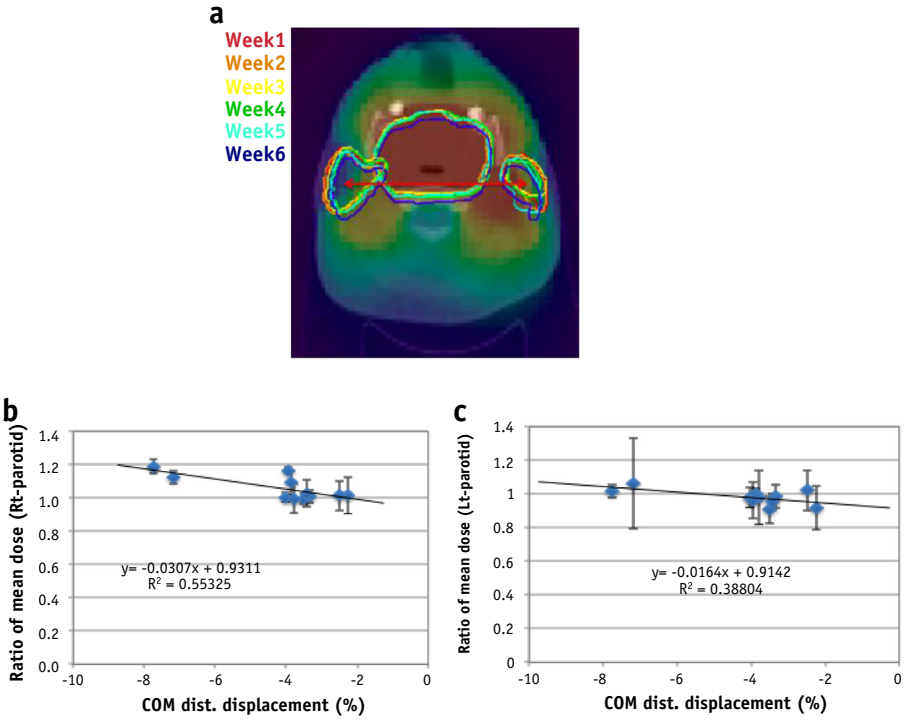


**Fig. 2.** (a) Contours of the targets and parotid glands assessed from the weekly kVCT scans overlaid on the planning dose distribution. Correlations between the displacement of the COM distance of the parotid glands and the mean dose variation at the end of treatment for the right (b [Rt]) and left (c [Lt]) parotid. COM = center of mass; dist. = distance; kVCT = kilovoltage computed tomography.

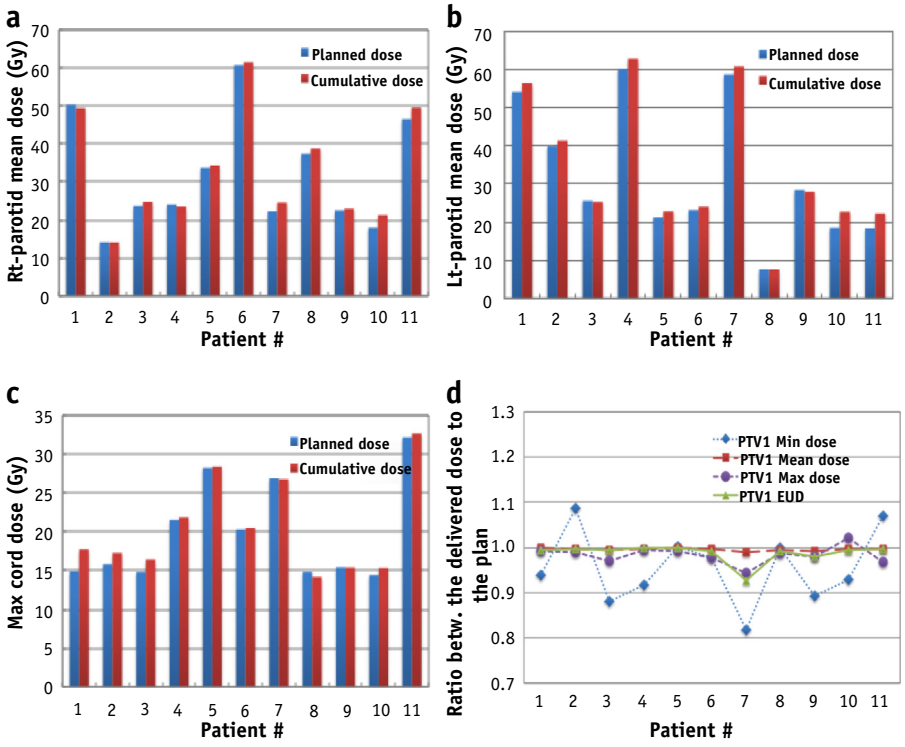


**Fig. 3.** Comparison of cumulative doses to planned doses for (a) right (Rt) parotid ($P = .03$), (b) left (Lt) parotid ($P = .006$), and (c) maximum cord doses compared to planned doses ($P = .18$). (d) Ratios of cumulative dose normalized to planned dose are shown for the PTV1. EUD = equivalent uniform dose; PTV = planning target volume.

Figure 4a shows the plan and the deformed structures on a weekly kVCT scan for a representative case. Figure 4b shows the planned dose distributions; Figure 4c shows the delivered dose distribution, and Figure 4d shows the calculated gamma distribution for those voxels with gamma >1 on the weekly kVCT scan. Such gamma maps can be used to identify areas that need closer inspection. At looser gamma criteria of 2 mm/2%, 71.7% (right parotid), and 89.7% (left parotid) volumes saw changes in dose but such dose changes were not extreme because the failure rates were minimal at 3%/3 mm (failure rates of 0% for the right and 1.4% for the left parotid). Comparison of the plan and delivered DVHs for the PTV1 and parotid glands are shown. Most of the gamma failure is around the surface of the patient, potentially due to weight loss and minor posture changes.

## Run-time analysis

The in-house dose deformation and accumulation tool achieved a fast calculation of 45 seconds for registering one weekly kVCT with a planning CT, including: (*1*) data resizing and resampling of approximately 2 seconds (resampled data dimensions: 200 × 200 × 50 voxels; resampled voxel dimensions: 1.95 × 1.95 × 3.0 mm); (*2*) the deformable image registration using optical flow registration algorithm of 20 seconds; (*3*) Jacobian analysis of 6 seconds; (*4*) gamma analysis of 5 seconds; and (*5*) other minor processes such as file reading and writing of 12 seconds (14).

## Discussion

A nearly real-time anatomic and dosimetric assessment and evaluation framework was presented that facilitates clinical decision making for ART by quantitatively accounting for plan quality degradation during the treatment course. A quantitative patient-specific biomechanical H&N anatomic model assembled using the conventional CT simulation (to account for subject-specific sub-anatomy locations), was used to register with routine on-board CT (to monitor the effects of posture/physiologic variations in gross treatment volume).

Progressive anatomical changes during the treatment resulted in substantially increased doses to the parotids and potential cold spots to the targets (1-4). The dosimetric degradation was a result of compounding factors including the percentage of volume and positional changes for the parotid glands, tumor shrinkage, patient weight loss, and others. Larger weight loss may have resulted in larger COM reduction of the parotid glands, which led to larger delivered doses to the parotids, but the correlation was not strong. Overall, our results are consistent with those of previous studies demonstrating dramatic patient anatomic changes during the radiation treatment for H&N cancer (9, 10, 16).

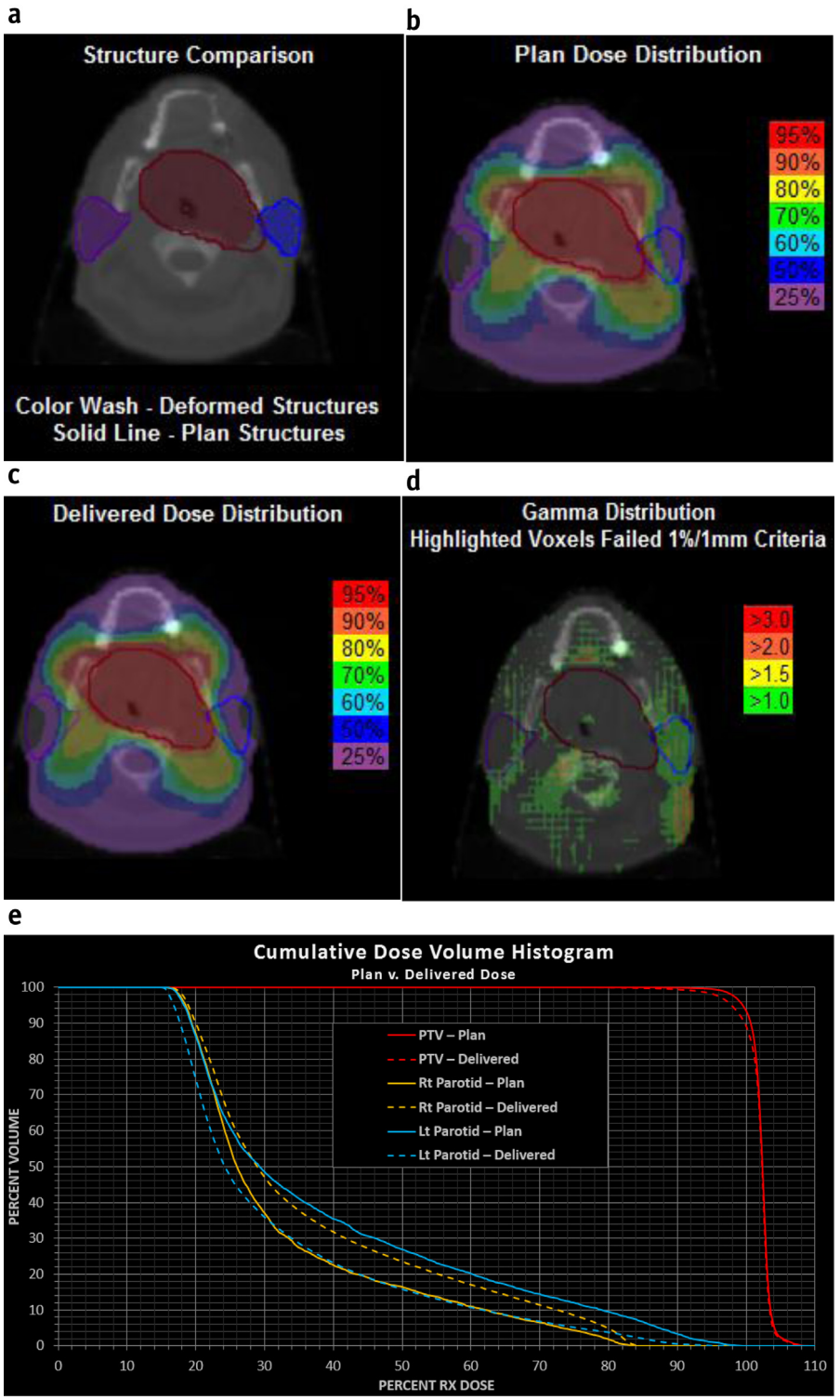


**Fig. 4.** (a) Planned and deformed structures on a weekly kVCT: (b) planned dose distributions; (c) delivered dose distribution; (d) calculated gamma distribution (gamma >1) overlaid on the weekly kVCT; (e) comparison of the planned to delivered DVHs for the PTV1 and parotid glands. DVH = dose-volume histogram; kVCT = kilovoltage computed tomography; Lt = left; PTV = planning tumor volume; Rt = right.

The concept of performing ART on a regular basis to quickly compensate for target underdoses and/or normal structure overdoses is appealing. However, its implementation is challenging because it is prohibitively labor intensive and time consuming to delineate and validate the target and OARs on a daily basis. ART usually involves altering the planned doses according to variations in patient anatomy. This relies on an accurate representation of the changing dose

distribution within the patient, which generally requires a full dose recalculation. To further reduce online replanning time, this work adopted a dose resampling or warping method (of the planned dose distribution) to assess 3-dimensional dose distribution at the time of treatment delivery. Dosimetric differences were validated against full dose recalculation for prostate and H&N ART by previous publications and proven to be well within ±5%. This is considered clinically acceptable and can be effective implementation in current clinical practice (17-20). This work however is in the context of the ICRU framework and the assumptions may not be applicable for low-margin probabilistic planning or highly targeted ablative therapy approaches. Furthermore, although the image quality for various on-board imaging modalities (such as kilovoltage and megavoltage cone beam CTs and megavoltage CT) was sufficient for bony landmark−based patient alignment purposes (2, 5, 21), they generally yield inferior image quality that could reduce the image registration, segmentation and dose deformation accuracy for adaptive planning. These limitations further underline the importance of an automated framework that is interobserver dependent and robust to different imaging qualities.

The next step is to integrate the framework into our clinical workflow to monitor the actual dose delivered to the primary targets and critical structures in a systematical manner and to flag large dose degradation between the planned and delivered dose distribution to trigger a detailed plan reviewing process and/or a potential plan adaption. Given a large number of H&N patients are being detected yearly (22) and the limited clinical resources, it is not realistic (and probably not necessary) to apply ART to all H&N patients. The presented tool may efficiently identify a subset of H&N patients for whom ART is most beneficial. In the long run, a longitudinal study for a randomized patient population may shed light to establish the standardized adaptive protocol.

## Conclusions

We demonstrated the feasibility of an ultrafast assessment and documentation framework for systemically monitoring the anatomic and dosimetric variations during the course of H&N treatment. The mean dose delivered to the target appeared to be consistent with the plan, whereas the cumulative EUDs for the PTV1 and cumulative dose to the OARs may be significantly different from the planned doses. The automated framework may offer timely interventions such as ART. Clinical implementation of this technology may lead to improved outcome.

## References


1. Barker JL, Garden AS, Ang KK, et al. Quantification of volumetric and geometric changes occurring during fractionated radiotherapy for head-and-neck cancer using an integrated CT/linear accelerator system. *Int J Radiat Oncol Biol Phys* 2004;59:960-970.
2. Gregorie V, Jeraj R, Lee JA, et al. Radiotherapy for head and neck tumors in 2012 and beyond: Conformal, tailored, and adaptive? *Lacent* 2012;4:e292-e300.
3. Wu Q, Chi Y, Chen P, et al. Adaptive replanning strategies accounting for shrinkage in head and neck IMRT. *Int J Radiat Oncol Biol Phys* 2009;75:924-932.
4. Lee C, Langen KM, Lu W, et al. Assessment of parotid gland dose changes during head and neck cancer radiotherapy using daily megavoltage computed tomography and deformation image registration. *Int J Radiat Oncol Biol Phys* 2008;71:1563-1571.
5. Qi XS, Hu AY, Lee SP, et al. Assessment of interfraction patient setup for head-and-neck cancer intensity modulated radiation therapy using multiple computed tomotherapy-based image guidance. *Int J Radiat Oncol Biol Phys* 2012;86:432-439.
6. Marks LB, Yorke ED, Jackson A, et al. Use of normal tissue complication probability models in the clinic. *Int J Radiat Oncol Biol Phys* 2010;75:S10-S19.
7. Low DA, Harms WB, Mutic S, et al. A technique for the quantitative evaluation of dose distributions. *Med Phys* 1998;25:656-661.
8. Worthy N, Wu Q. Dosimetric assessment of rigid setup error by CBST for HN-IMRT. *J Appl Clin Med Phys* 2010;11:38-53.
9. Schwartz DL, Garden AS, Thomas J, et al. Adaptive radiotherapy for head-and-neck cancer: Initial clinical outcomes from a prospective trial. *Int J Radiat Oncol Biol Phys* 2012;83:986-993.
10. Castadot P, Geets X, Lee JA, et al. Assessment by a deformable registration method of the volumetric and positional changes of target volumes and organs at risk in pharyngo-laryngeal tumors treated with concomitant chemo-radiation. *Radiother Oncol* 2010;95:209-217.
11. Castadot P, Lee JA, Geets X, et al. Adaptive radiotherapy of head and neck cancer. *Semin Radiat Oncol* 2010;20:84-93.
12. Nishi T, Nishimura Y, Shibata T, et al. Volume and dosimetric changes and initial clinical experience of a two-step adaptive intensity modulated radiation therapy (IMRT) scheme for head and neck cancer. *Radiother Oncol* 2013;106:85-89.
13. Chen AM, Daly ME, Cui J, et al. Clinical outcomes among patients with head and neck cancer treated by intensity-modulated radiotherapy with and without adaptive preplanning. *Head Neck* 2014;1:1-6.
14. Neylon J, Qi XS, Sheng K, et al. A GPU based high-resolution multilevel biomechanical head and neck model for validating deformable image registration. *Med Phys* 2015;42:232-243.
15. Min Y, Neylon J, Shah A, et al. 4D-CT lung registration using anatomy based multi-level multi-resolution optical flow analysis and thin plate splines. *Int J Comput Assist Radiol Surg* 2014;9:875-889.
16. Ahn PH, Chen CC, Ahn AI, et al. Adaptive planning in intensity-modulated radiation therapy for head and neck cancers: Single-institution experience and clinical implications. *Int J Radiat Oncol Biol Phys* 2011;80:677-685.
17. Smyth G, McCallum HM, Lambet EL, et al. A dose distribution overlay technique for image guidance during prostate radiotherapy. *Br J Radiol* 2008;81:890-896.
18. Sharma M, Weiss E, Siebers JV. Dose deformation-invariance in adaptive prostate radiation therapy: Implication for treatment solutions. *Radiat Oncol* 2012;105:207-213.
19. Pukala J, Staton R, Langen K. What is the importance of dose recalculation for adaptive radiotherapy dose assessment? *Med Phys* 2012;39:3699-3700.
20. Pukala J, Gray T, Meeks SL, et al. Adaptive radiation therapy replanning for head-and-neck cancers and the dosimetrix benefit to the parotid glands. *Int J Radiat Oncol Biol Phys* 2013;87:S713-S714.
21. Hong TS, Tome WA, Chappell RJ, et al. The impact of daily setup variations on head and neck intensity modulated radiation therapy. *Int J Radiat Oncol Biol Phys* 2005;61:779-788.
22. National Cancer Institute. Head and neck cancers. Available at: http://www.cancer.gov/cancertopics/factsheet/Sites-Types/head-and-neck. Accessed August 20, 2013.